TECHNICAL REPORT R-76

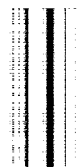## CALCULATED EFFECTS OF BODY SHAPE ON THE BOW-SHOCK OVERPRESSURES IN THE FAR FIELD OF BODIES IN SUPERSONIC FLOW

By DONALD L. LANSING

Langley Research Center
Langley Field, Va.

TECHNICAL REPORT R-76

CALCULATED EFFECTS OF BODY SHAPE ON THE BOW-SHOCK OVERPRESSURES IN THE FAR FIELD OF BODIES IN SUPERSONIC FLOW

By Donald L. Lansing

SUMMARY

The theory developed by G. B. Whitham (Communications on Pure and Applied Mathematics, August 1952) for the supersonic flow about bodies in uniform flight in a homogeneous medium is reviewed and an integral which expresses the effect of body shape upon the flow parameters in the far field is reduced to a form which may be readily evaluated for arbitrary body shapes. This expression is then used to investigate the effect of nose angle, fineness ratio, and location of maximum body cross section upon the far-field pressure jump across the bow shock of slender bodies. Curves are presented showing the variation of the shock strength with each of these parameters. It is found that, for a wide variety of shapes having equal fineness ratios, the integral has nearly a constant value. Hence, to a first order, the pressure jump in the far field is independent of the shape and depends only upon the fineness ratio.

INTRODUCTION

Airplanes operating at supersonic speeds may produce shock waves of considerable intensity at ground level. The shock pattern travels with the airplane, sometimes sweeping over large populated areas on the ground below. The atmosphere experiences a sudden increase in pressure as the shock wave passes through it. This pressure jump across the shock is heard by the observer as a sharp explosive-type sound, the so-called "sonic boom." Under some circumstances damage may result to building components. Thus, the sonic boom has become a serious operating problem and reliable theoretical prediction of the magnitude of sonic booms has become increasingly desirable. A variety of conditions—such as,

airplane size, speed, altitude, flight path, winds, and atmospheric nonuniformities—are known to affect the strength of a sonic boom. In the present paper the effects of body geometry are investigated.

One of the more promising theoretical methods for predicting the strength of shock waves from aircraft at large distances appears to be that developed by G. B. Whitham (ref. 1). This theory is a rather lengthy modification of the linear supersonic theory of slender bodies which predicts the location and strength of the shock waves emanating from a body in addition to the surface pressures and wave drag. Whitham's results, which apply to thickness effects only, may be conveniently separated into two parts: the prediction of the complicated pressures and shock interactions near the body and the greatly simplified flow pattern at sufficiently large distances. Whitham shows that the calculation of the pressure jump across the bow shock in the far field requires only a single formula which gives the magnitude of the discontinuity in terms of the flight Mach number, distance from the flight path, and a coefficient which depends upon body shape and must be evaluated for each configuration under study.

Whitham's theory has considerable theoretical and experimental verification. When applied to two-dimensional problems the method gives a first approximation to the result previously obtained by K. O. Friedrichs (ref. 2). The theoretically predicted far-field strength and decay of the bow shock of a supersonic body agrees favorably with the experimental evidence gathered from studies of bullets in flight (ref. 3), wind-tunnel investigations (ref. 4), and flight tests

of full-scale airplanes (refs. 5, 6, and 7). On the basis of these results it is felt that Whitham's theory will serve as a useful guide in predicting the trends of the overpressures associated with sonic booms.

The present paper is concerned with the effect of body shape and fineness ratio upon the thickness-induced pressures in the far field. For background the fundamental hypothesis upon which Whitham's work is founded is given, the physical basis for the theory is discussed, and then a brief development of the equations for the far-field conditions is given. The expression for the effect of body shape upon the flow parameters in the far field is reduced to a convenient form and then applied to a number of families of body shapes chosen to investigate the effect of fineness ratio, location of maximum thickness, and nose angle on the pressure jump across the bow shock. The reader interested only in the results may proceed directly to the application.

SYMBOLS

C_b body-shape constant defined in equation (24)

$$F(y)=\frac{1}{2\pi}\int_0^y \frac{S''(\xi)}{\sqrt{y-\xi}}\,d\xi$$

$$I(y)=\int_0^y F(y)\,dy$$

I_{max} largest value which $I(y)$ assumes for given body

l length of body

M free-stream Mach number

n integer

p ambient pressure

p_∞ free-stream pressure

$\Delta p=p-p_\infty$

R radius of body-wake combination

R_{max} maximum radius of body-wake combination

$R'(0)$ nose semiangle

S cross-sectional area, πR^2

U_∞ free-stream velocity

x,r cylindrical coordinates; x is measured along body axis downstream from nose, r is radial coordinate measured perpendicular to x

$(x/l)_{max}$ distance from nose at which radius of body is R_{max}

y,ξ,η variables

$\beta=\sqrt{M^2-1}$

γ polytropic index, 1.4

Δ interval size for numerical integration

θ local direction of flow

μ local Mach angle

φ velocity potential

Subscripts:

b body geometry

w wake geometry

DESCRIPTIVE OUTLINE OF WHITHAM'S WORK

WHITHAM'S BASIC HYPOTHESIS

The theory of reference 1 is a modification of the linear supersonic theory of nonlifting slender bodies. The basic idea on which the theory is based is that the failure of linear theory away from the body surface and near shocks is due not so much to incorrect prediction of physical quantities along the characteristics but to improper placing of the characteristic curves in the flow field. More precisely, the fundamental assumption upon which Whitham's work is based may be stated as follows. Linear theory gives a first approximation to the entire flow provided the value it predicts for any physical quantity at a given distance from the body axis on a straight Mach line through a given point on the body surface is interpreted as the value at the given distance from the axis on the exact characteristic curve pointing downstream from the given point on the body surface. Thus, the failure of linear theory, in which the characteristics are straight Mach lines, may be remedied by introducing a more exact expression for the form of the characteristics which takes their bending into account. The curved characteristics may converge in various regions of the flow field indicating the presence of shocks, and may diverge in other regions of the flow indicating expansions.

THE PRESSURE AS PREDICTED BY LINEAR THEORY

The physical implications of this basic hypothesis may be seen with the aid of figures 1 and 2. Figure 1 shows the characteristic field and a typical pressure trace of a simple slender-body—wake combination as predicted by linear theory. The wake, shown by the dashed curves, converges near the body and rapidly thins to a cylinder of approximately constant cross section. The characteristics—such as, AB, EF, and WZ—issuing from various points along the surface and the
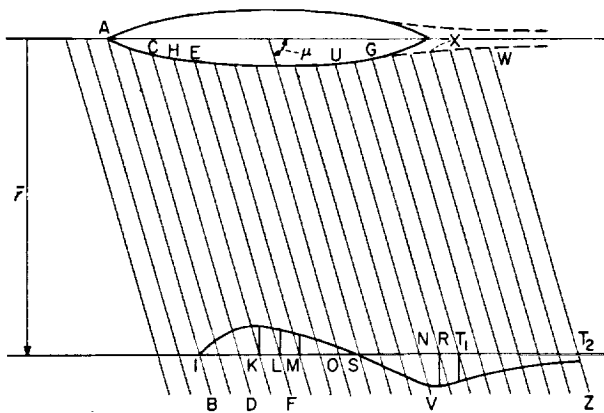
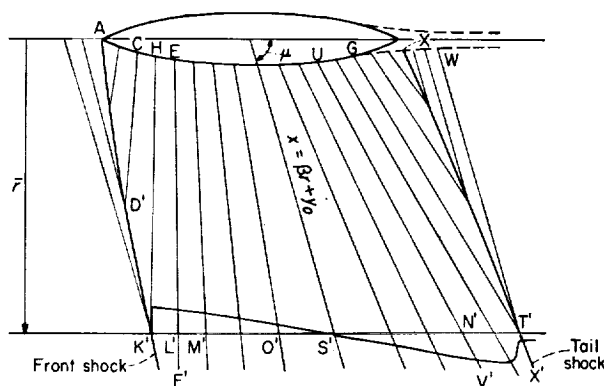FIGURE 1.—Characteristics and pressure as predicted by linear theory.

FIGURE 2.—Characteristics and pressure as predicted by the modified theory.

characteristics in the upstream uniform flow are a series of parallel straight lines, the Mach lines $x-\beta r=$ Constant, which make an angle $\mu=\sin^{-1}\dfrac{1}{M}$ with the body axis. Let I, K, L, . . . R, T_1, T_2 represent various field points along a line parallel to the body axis but at some given distance, say $\bar{r}$, from it. The atmosphere experiences a gradual compression as it passes through the forward portion of the characteristic field associated with the body (between I and K), and the ambient pressure begins to rise above free-stream pressure. After reaching maximum compression at K the atmosphere expands (between K and R) and the ambient pressure falls to some minimum value at R which is below free-stream pressure. Between the maximum and minimum values the ambient pressure becomes equal to the free-stream pressure at S. After the ambient pressure reaches a minimum at R the atmosphere is again com-

pressed; the ambient pressure slowly rises to free-stream pressure.

THE CHARACTERISTICS AND SHOCKS IN THE MODIFIED THEORY

Conspicuously absent from linear theory are shock waves, clearly visible in photographs of projectiles in flight, and their associated pressure discontinuities. The first step in introducing the shock waves into the flow consists in deriving a more accurate expression for the shape of the characteristics and then replacing the Mach lines of linear theory by these more correct curves. The shape of the characteristics depends upon the local flow direction and the local speed of sound. The variation of these quantities from their main-stream values is neglected in linear theory. In the approximation used by Whitham (ref. 1) the characteristics in the uniform upstream flow remain unchanged from the straight Mach lines of linear theory, whereas the characteristics issuing from the surface of the body and wake are curved, their exact shape depending upon the cross-sectional-area development of the body. There will, however, be one straight characteristic issuing from a point near the center of the body. This characteristic extends to infinity, and everywhere along it the ambient pressure is equal to the free-stream pressure. The equation of this line is given by $x-\beta r=y_o$ where the exact value of y_o depends upon the body shape. In general, the curved characteristic through a point on the body surface is upstream from the Mach line through the same point in those regions for which the ambient pressure is more than the free-stream pressure and is downstream from the Mach line in regions where the ambient pressure is less than the free-stream pressure.

As a result of this varying shape and curvature, the characteristics tend to run together and overlap in some regions of the flow. In such regions shock waves are introduced by the "angle" condition: if two regions of supersonic flow are separated by a shock then, to the first order in the strength, the direction of the shock bisects the Mach direction of the two regions of flow. (The Mach direction at a point is the outward direction making the local Mach angle with the local flow direction.) The resulting shock waves appear in the flow in such a manner as to cut off the characteristics before they overlap.

THE PRESSURE AS PREDICTED BY THE MODIFIED THEORY

The modifications of the flow field in figure 1 are shown in figure 2. In this figure the points $C, H, E, \ldots W$ correspond to the points similarly labeled in figure 1. Associated with each of these points there is a curved characteristic such as $C'D'$, EF', UV' which replaces the corresponding Mach line of linear theory, CD, EF, and UV in figure 1. The shocks are shown as the curves labeled $AD'K'$ and $XT'X'$. The Mach line $x-\beta r=y_o$ effectively separates the characteristic field into two distinct portions, one associated with each of the two shock waves. In order to obtain the pressure at any point in the field, the basic hypothesis stated previously is used. Let $K', L', M', \ldots T'$ represent field points along a line parallel to the body axis and at the given distance $\bar{r}$ from it. Let the points be chosen so that curved characteristics which pass through them intersect the body at the same places as do the Mach lines through the points $K, L, M, \ldots T_1, T_2$ in figure 1. Then, the basic hypothesis states that the pressure at $L', M', \ldots S', N'$ is the same as the pressure predicted by linear theory at the points $L, M, \ldots S, N$ in figure 1. In this manner the pressure may be found at any point not on a shock wave.

Any point on a shock wave is the meeting place of two characteristics each carrying a different pressure, and hence a sudden increase in pressure is experienced as a shock wave is crossed. In figure 2 the upstream Mach line through K' carries with it the free-stream pressure, whereas the downstream curved characteristic HK' carries the same pressure as point K in figure 1. Thus, a pressure jump equal to Δp at K is experienced as the shock is crossed at K'. This method of determining the pressure discontinuity along the shocks shows that the strength of the bow shock at first increases until maximum strength is reached at some distance from the body axis, and thereafter decays with distance. Similarly, at T' on the rear shock, where the curved characteristics through G and W on the body-wake surface meet, the excess pressure on the upstream side of the shock is the same as that at T_1; the excess pressure downstream is the same as that at T_2. The pressure jump as the shock is crossed at T' is again the difference in these two pressures.

For a body shape which gives rise to a number of regions of positive and negative overpressure, the characteristic field and the resulting shock system will, of course, be far more complicated than that described here. However, it is important to notice that the modifications of linear theory described above tend to smooth out the flow pattern between the shocks by "pushing" local irregularities away from the Mach line $x-\beta r=y_o$ and into the shocks as the distance from the body increases. Thus, although a system of more than two shocks may appear in the neighborhood of the body, in general these will coalesce at some distance leaving only two shocks extending to large distances. In the far field there is an abrupt pressure rise across the front shock, a nearly linear decline in pressure between the shocks, and a recompression at the rear shock to nearly the free-stream pressure. This is the typical N-wave pressure pulse associated with the sonic boom.

FURTHER ASSUMPTIONS AND RESTRICTIONS TO THE THEORY

In addition to the basic hypothesis discussed, the assumptions from which Whitham's theory proceeds are the usual requirements of linear theory—that is, the body is axisymmetric, slender, and pointed at the nose. The upstream field is uniform with Mach number sufficiently in excess of 1.0 for the bow shock to be attached. The flow within the wake is not determined; however, the mean boundary of the wake associated with a given body is assumed known. The wake is then treated as a solid extension of the body; that is, there is no flow across the assumed wake boundary. The radius of the body-wake combination must be continuous although the slope may be discontinuous.

Under these assumptions, reference 1 gives a first-order approximation to the entire pressure field due to thickness. A method is described for determining the location of the shocks, the pressure jump across the shocks, the pressure signature between the shocks, and the flow field behind the body outside the wake.

If the projectile is not axisymmetric or has a small fineness ratio the shock pattern and pressures in the near field may differ appreciably from those of a slender symmetric body to which the theory is applicable. However, at sufficiently large distances from such a body the disturbances will be small and the theory may be used to give useful information of the far-field conditions. For a parabolic body of fineness ratio 5 the trend of the

far-field decay of the bow-shock overpressure as predicted by theory agrees well with experimental results (ref. 4).

The assumption that the body is pointed at the nose, a usual requirement in linear theory is implicit in Whitham's equations for the perturbation velocities. Erroneous results may be obtained if the theory is applied to a blunt shape. For example, the theory is inapplicable to an elliptical body (major axis in stream direction) although experimental work (ref. 4) shows that the far-field pressures are essentially the same as those for a parabolic body of the same fineness ratio.

At low supersonic Mach numbers the bow shock will be detached. A region of subsonic flow then exists in the vicinity of the body nose. The shock in the neighborhood of the nose is then considerably stronger than in the case of an attached shock. It is difficult to justify, on a theoretical basis, the use of Whitham's equation in this instance. However, flight test data (ref. 5) obtained at low supersonic Mach numbers indicate that reasonably good agreement is obtained in this case. A detached shock also exists ahead of a blunt-nose projectile. There is a real difficulty in applying the results to such a shape as already noted for the elliptic body.

THE BASIC EQUATIONS OF THE MODIFIED THEORY

For the sake of completeness a brief derivation is given of the equations for the far-field conditions pertinent to the front shock. The numerical evaluation of the equation obtained for the pressure discontinuity will be dealt with in some detail subsequently. Certain general results, applicable to a variety of axisymmetric problems, are first derived, and then the salient features of the far field of a smooth body are obtained by introducing the appropriate approximations for large values of r.

From the linearized theory of supersonic flow it is known (ref. 8) that the form of the perturbation potential appropriate to a nonlifting body of revolution is

$$\varphi(x, r) = -\int_0^{x-\beta r} \frac{f(t)}{\sqrt{(x-t)^2-\beta^2 r^2}}\, dt$$

where the function $f(t)$ is to be determined from the boundary condition of tangential flow at the body surface. The perturbation velocities are then obtained by differentiating φ:

$$\left.\begin{aligned}
u &= \frac{\partial\varphi}{\partial x} = -\frac{f(0)}{\sqrt{x^2-\beta^2 r^2}} - \int_0^{x-\beta r} \frac{f'(t)}{\sqrt{(x-t)^2-\beta^2 r^2}}\, dt \\
v &= \frac{\partial\varphi}{\partial r} = \frac{x}{r}\frac{f(0)}{\sqrt{x^2-\beta^2 r^2}} + \frac{1}{r}\int_0^{x-\beta r} \frac{(x-t)f'(t)}{\sqrt{(x-t)^2-\beta^2 r^2}}\, dt
\end{aligned}\right\} \quad (1)$$

For axisymmetric slender smooth bodies, $S(x)$ and $S'(x)$ continuous, the condition of tangential flow requires that $f(x) = \frac{U_\infty}{2\pi} S'(x)$ where $S(x)$ is the cross-sectional area and U_∞ is the free-stream velocity. For small disturbances the body must be pointed at the nose, $S'(0)=0$; hence, $f(0)=0$ and only the integral terms need be retained in equations (1).

Following the basic hypothesis outlined in the previous section, Whitham replaces $x-\beta r$, the characteristic variable of linear theory, by $y(x,r)$. The function $y(x,r)$ is determined from the condition that $y(x,r)=$ Constant be a characteristic curve; that is, along the curve

$$\frac{dx}{dr} = \cot(\mu+\theta) \quad (2)$$

where μ is the local Mach angle and θ is the local direction of flow. The characteristic variable y is defined uniquely by the convention that at any point on the body surface y is the value of the linear characteristic $x-\beta r$ which passes through that point. Thus, the equation $y=x_o-\beta r_o$ defines a nonlinear characteristic curve which passes through the point x_o, r_o on the body surface. For bodies of large fineness ratio $l/2R_{max}$, $\beta R \ll x$ and $y \approx x$. Hence, a convenient interpretation of the variable y is that it is the horizontal distance from the nose at which the extended characteristic curve intercepts the body axis.

The basic results of the modified theory regarding the pressure at any point in the field, the shape of the curved characteristics, and the location of the front shock may be obtained as follows. In equations (1) (where now $f(0)=0$), if x is replaced by $y+\beta r$ and the integrands are approximated for small values of $y/\beta r$, the following expressions are obtained:

$$\left.\begin{aligned}
\frac{u}{U_\infty} &\approx -\frac{F(y)}{\sqrt{2\beta r}} \\
\frac{v}{U_\infty} &\approx -\beta\frac{u}{U_\infty}
\end{aligned}\right\} \quad (3)$$

in which

$$F(y) = \frac{1}{2\pi} \int_0^y \frac{S''(t)}{\sqrt{y-t}} \, dt$$

In the undisturbed flow ahead of the body $F(y) \equiv 0$. The pressure at any point in the field is then given by equations (3) and the result of linear theory as

$$\frac{\Delta p}{p_\infty} = -\gamma M^2 \frac{u}{U_\infty} = \frac{\gamma M^2}{\sqrt{2\beta}} \frac{F(y)}{r^{1/2}} \qquad (5)$$

The differential equation for the characteristics, equation (2), may be approximated to the first order in u/U_∞ and v/U_∞ as

$$\frac{dx}{dr} = \beta + \sqrt{\frac{\beta}{2}} k \frac{u}{U_\infty} - M^2 \left(\frac{v}{U_\infty} + \beta \frac{u}{U_\infty} \right) \qquad (6)$$

where $k = \dfrac{M^4(\gamma+1)}{\sqrt{2} \beta^{3/2}}$. When equation (3) is used, equation (6) becomes

$$\frac{dx}{dr} = \beta - kF(y) \frac{1}{2\sqrt{r}} \qquad (7)$$

If equation (7) is integrated along the characteristic

$$y = x_0 - \beta r_0 \qquad (8)$$

from the point x_0, r_0 on the body surface to a field point x, r, it follows that at large distances on the characteristic the following equation must hold:

$$x = \beta r - kF(y)r^{1/2} + y \qquad (9)$$

Equations (8) and (9) constitute a parametric representation of the curved characteristics. The two equations may also be interpreted as defining the value of y, and hence of $F(y)$, appropriate to any field point x, r.

With the shape of the characteristics known, the "angle" property which must be satisfied along a shock is then applied to determine the location of the front shock. In terms of the parameter y, it is found that along the front shock one must have

$$x = \beta r + y - kF(y)r^{1/2} \qquad (10)$$

and

$$r^{1/2} = \frac{2}{kF(y)^2} \int_0^y F(\eta) d\eta \qquad (11)$$

The function $F(y)$ defined by equation (4) is of fundamental importance in the entire theory. Equation (5) shows that, at a given radial distance from the body axis, the longitudinal variation in pressure is proportional to $F(y)$. The atmosphere undergoes compression over those portions of the body for which $F'(y) > 0$ and expansion where $F'(y) < 0$. In general, a shock is formed for each value of y for which $F''(y) = 0$ and $F'(y) > 0$ hold simultaneously. These shocks usually run together at some distance from the body in such a manner that only two shocks remain in the far field. If the ultimate cross-sectional area of the wake $S_w(\infty)$ is finite the function $F(y)$ has the following properties and physical interpretations:

(a) The initial compression at the nose:

$$F(y) \sim 2[R'(0)]^2 y^{1/2} \quad \text{as} \quad y \to 0$$

(b) Recompression outside the wake:

$$F(y) \sim -\frac{S_w(\infty)}{4\pi} y^{-3/2} \quad \text{as} \quad y \to \infty$$

(c) The balance of compression and expansion:

$$\int_0^\infty F(\eta) d\eta = 0 \qquad (12)$$

(d) Reexpansion behind a closed body with no wake, $S_w(\infty) = 0$:

$$F(y) \sim \frac{3V}{8\pi} y^{-5/2} \quad \text{as} \quad y \to \infty$$

where V is the volume of the projectile.

FURTHER SIMPLIFICATIONS APPROPRIATE FOR LARGE DISTANCES

From these general results the simplified equations for the conditions at the front shock are obtained which are sufficiently accurate in the field at large distances from the body-wake combination. This is the region of greatest concern in the prediction of sonic-boom intensities. Since the expressions to be obtained are asymptotic results for large values of r, they should not be expected to give valid results in the neighborhood of the body. The conditions under which the results are valid are restated: The body is assumed to be axisymmetric, slender, and pointed at the nose ($S_b(0) = S_b'(0) = 0$); the projectile-wake surface is smooth ($S(x)$ and $S'(x)$ continuous everywhere); and the ultimate cross section of the wake $S_w(\infty)$ is finite.

In addition, it is assumed, as is generally the case, that only two shocks reach into the far field. A thorough discussion of the structure of the near field, the circumstance leading to the appearance of three or more shocks in the far field, and the methods for dealing with such problems as the infinite slender cone and bodies with discontinuous slope, such as the double cone, are given in reference 1. These problems require more general techniques than are needed for the body shapes considered in this paper.

The far-field approximations depend upon the fact that between the shocks the only characteristics reaching to large distances are those for which $y \approx y_o$ (fig. 2). The characteristic defined by $y = y_o$ is a straight line and, therefore, from equation (9), $F(y_o) = 0$. Figure 2 also indicates that in the far field large changes in the radial distance along the shocks are equivalent to very small changes in y. Hence, with little loss of accuracy, equation (11) becomes

$$F(y) = \sqrt{\frac{2}{k} \frac{1}{r^{1/4}}} \sqrt{\int_0^{y_o} F(\eta) d\eta} \tag{13}$$

From equations (13) and (10), the equation for the location of the front shock becomes

$$x - \beta r - y_o = -r^{1/4} \sqrt{2k \int_0^{y_o} F(\eta) d\eta} \tag{14}$$

From equations (13) and (5), the pressure discontinuity across the shock is

$$\frac{\Delta p}{p_\infty} = \frac{2^{1/4} \gamma}{\sqrt{\gamma + 1}} \frac{\beta^{1/4}}{r^{3/4}} \sqrt{\int_0^{y_o} F(\eta) d\eta} \tag{15}$$

Equation (15) is the fundamental equation widely used in predicting sonic-boom overpressures at large distances.

The pressure at any point between the shocks may be determined by approximating equation (9) as

$$F(y) = \frac{\beta r + y_o - x}{k r^{1/2}}$$

and combining with equation (5) to obtain

$$\frac{\Delta p}{p_\infty} = \frac{\gamma \beta}{(\gamma + 1) M^2} \frac{1}{r} (\beta r - x + y_o)$$

from which for fixed large values of r the pressure

between the shock falls linearly at a constant rate independent of the body shape.

NUMERICAL EVALUATION OF THE INTEGRAL FOR THE PRESSURE JUMP IN TERMS OF CROSS-SECTIONAL-AREA DISTRIBUTION

It is to be noticed that the detailed behavior of the function $F(y)$ is of no concern in the prediction of the magnitude and decay of the pressure jump across the bow shock in the far field. From equation (15) it can be seen that only the value of the expression $\int_0^{y_o} F(\eta) d\eta$ is required. The value of this definite integral depends upon shape of the body-wake combination under investigation (as shown by eq. (4)) and, of course, varies from one shape to another.

The value of the upper limit y_o is determined from the condition that the integral

$$I(y) = \int_0^y F(\eta) d\eta$$

is a maximum at $y = y_o$. A necessary condition for a maximum at $y = y_o$ is

$$\frac{dI}{dy} = F(y) = 0$$

hence, y_o is a root of the equation $F(y) = 0$. However, the appropriate root is not necessarily the first solution of $F(y) = 0$ (excluding $y_o = 0$) as has been indicated in some of the literature concerned with Whitham's method. One must integrate to that root which maximizes the integral $I(y)$ in order to account for the total strength of any subsidiary shocks which may have run together near the body to form a single intensified bow shock reaching to large distances. Since the total expansion and compression must balance (eq. (12)), there is always a root satisfying the required conditions for body-wake combinations whose ultimate radius is finite.

The expression for $I(y)$ will now be reduced to a form which avoids determining $F(y)$ explicitly. The result to be obtained allows rapid calculation of the required maximum value and is particularly useful in dealing with shapes for which no analytic expression is available or for which the analytic expression is tedious to handle in an exact manner.

Write equation (4) in the form

$$F(\eta) = \frac{2}{2\pi} \frac{d}{d\eta} \int_0^\eta S''(\xi) \sqrt{\eta - \xi}\, d\xi$$

Then, the following expression for $I(y)$ is easily obtained by integration:

$$I(y)=\int_0^y F(\eta)d\eta=\frac{2}{2\pi}\int_0^y S''(\xi)\sqrt{y-\xi}\,d\xi$$

Integrating by parts and using the condition $S'(0)=0$ yields

$$I(y)=\frac{1}{2\pi}\int_0^y \frac{S'(\xi)}{\sqrt{y-\xi}}\,d\xi$$

This integral will now be evaluated numerically by using an equal-interval Simpson's rule. This rule requires that the upper limit y be an even multiple of the interval size which will be denoted by Δ. For the shapes treated in this paper $I(y)$ is a well-behaved function which presents no difficulty if the integration is carried out analytically. However, if the integral is to be evaluated numerically one must take care in handling the singularity of the integrand at the upper limit. For this purpose it is convenient to separate the integral into two parts

$$I(y)=\frac{1}{2\pi}[I_1(y)+I_2(y)]$$

where

$$I_1(y)=\int_0^{y-2\Delta}\frac{S'(\xi)}{\sqrt{y-\xi}}\,d\xi$$

$$I_2(y)=\int_{y-2\Delta}^y \frac{S'(\xi)}{\sqrt{y-\xi}}\,d\xi$$

If the condition $S(0)=0$ is used, $I_1(y)$ may be integrated by parts to obtain

$$I_1(y)=\frac{S(y-2\Delta)}{\sqrt{2\Delta}}-\frac{1}{2}\int_0^{y-2\Delta}\frac{S(\xi)}{(y-\xi)^{3/2}}\,d\xi \quad (16)$$

Applying Simpson's rule to the integral remaining in equation (16) yields

$$I_1(y)=\frac{1}{6\sqrt{\Delta}}\left[\frac{11\sqrt{2}}{4}S(y-2\Delta)-\frac{4}{3^{3/2}}S(y-3\Delta)\right.$$
$$\left.-\frac{2}{4^{3/2}}S(y-4\Delta)-\frac{4}{5^{3/2}}S(y-5\Delta)-\ldots\right] \quad (17)$$

The number of terms in equation (17) depends upon the values chosen for y and Δ; however,

it may be noted that the last term always involves $S(0)$ which is zero.

The integral $I_2(y)$ may similarly be integrated by parts:

$$I_2(y)=\left[\frac{S(\xi)}{\sqrt{y-\xi}}-\frac{1}{2}\int\frac{S(\xi)}{(y-\xi)^{3/2}}\,d\xi\right]_{y-2\Delta}^y \quad (18)$$

The integral in equation (18) is equivalent to the expression

$$\int\frac{S(\xi)+(y-\xi)S'(y)-S(y)}{(y-\xi)^{3/2}}\,d\xi$$
$$-S'(y)\int\frac{1}{\sqrt{y-\xi}}\,d\xi+S(y)\int\frac{1}{(y-\xi)^{3/2}}\,d\xi$$

which may be simplified by integrating the last two terms as follows:

$$\int\frac{S(\xi)+(y-\xi)S'(y)-S(y)}{(y-\xi)^{3/2}}\,d\xi$$
$$+2S'(y)\sqrt{y-\xi}+2\frac{S(y)}{\sqrt{y-\xi}} \quad (19)$$

Thus, substituting equation (19) into equation (18) gives

$$I_2(y)=\left[\frac{S(\xi)-S(y)}{\sqrt{y-\xi}}-S'(y)\sqrt{y-\xi}\right.$$
$$\left.-\frac{1}{2}\int\frac{S(\xi)+(y-\xi)S'(y)-S(y)}{(y-\xi)^{3/2}}\,d\xi\right]_{y-2\Delta}^y$$
$$=-\frac{1}{2}\int_{y-2\Delta}^y\frac{S(\xi)+(y-\xi)S'(y)-S(y)}{(y-\xi)^{3/2}}\,d\xi$$
$$+S'(y)\sqrt{2\Delta}+\frac{S(y)}{\sqrt{2\Delta}}-\frac{S(y-2\Delta)}{\sqrt{2\Delta}} \quad (20)$$

The integrand of the integral appearing in equation (20) is finite over the range of integration and vanishes at the upper limit. Evaluating this integral by using a three-point Simpson's rule gives

$$I_2(y)=\frac{11\sqrt{2}-8}{12}\sqrt{\Delta}S'(y)-\frac{1}{6\sqrt{\Delta}}\left[\frac{13\sqrt{2}}{4}S(y-2\Delta)\right.$$
$$\left.+4S(y-\Delta)-\frac{13\sqrt{2}+16}{4}S(y)\right] \quad (21)$$

If the results obtained for $I_1(y)$ and $I_2(y)$ (eqs.

(17) and (21)) are combined, $I(y)$ is found to be

$$I(y) = \frac{1}{2\pi} \left\{ \frac{11\sqrt{2}-8}{12} \sqrt{\Delta} S'(y) \right.$$

$$+ \frac{1}{6\sqrt{\Delta}} \left[\left(\frac{13\sqrt{2}+16}{4} \right) S(y) - 4S(y-\Delta) \right.$$

$$- \frac{2}{2^{3/2}} S(y-2\Delta) - \frac{4}{3^{3/2}} S(y-3\Delta)$$

$$\left. \left. - \frac{2}{4^{3/2}} S(y-4\Delta) - \ldots \right] \right\} \quad (22)$$

The number of terms in the series in brackets depends upon y and Δ and terminates with the term involving $S(0)$, which is zero. If no analytic expression is available for $S(y)$, the $S'(y)$ term in equation (22) may be eliminated by introducing the approximation

$$S'(y) = \frac{S(y+\Delta) - S(y-\Delta)}{2\Delta}$$

The expression for $I(y)$ may then be written

$$I(y) = -\frac{1}{2\pi} \frac{1}{6\sqrt{\Delta}} \left[\frac{8-11\sqrt{2}}{4} S(y+\Delta) - \frac{13\sqrt{2}+16}{4} S(y) \right.$$

$$+ \frac{8+11\sqrt{2}}{4} S(y-\Delta) + \frac{2}{2^{3/2}} S(y-2\Delta)$$

$$+ \frac{4}{3^{3/2}} S(y-3\Delta) + \frac{2}{4^{3/2}} S(y-4\Delta)$$

$$\left. + \frac{4}{5^{3/2}} S(y-5\Delta) + \ldots \right] \quad (23)$$

Equation (23) is the working form desired from which the maximum of $I(y)$ may be readily found. It is particularly appropriate for application to shapes which cannot be readily expressed analytically since it involves only the cross-sectional-area distribution. In application a rough calculation is first made to isolate the positive peaks in $I(y)$. More than one peak may occur. The peak regions are then investigated more thoroughly to determine which is the absolute maximum. The pressure discontinuity across the bow shock of the body is then simply

$$\frac{\Delta p}{p_\infty} = \frac{2^{1/4}\gamma}{\sqrt{\gamma+1}} \frac{\beta^{1/4}}{r^{3/4}} \sqrt{I_{max}}$$

It is convenient to normalize $S(y)$ to its maximum value S_{max}, and normalize the interval size Δ to

the body length l. If $I_{max} = \frac{S_{max}}{\sqrt{l}} \bar{I}_{max}$, the formula for the pressure jump becomes

$$\frac{\Delta p}{p_\infty} = \frac{\beta^{1/4}}{\left(\frac{r}{l}\right)^{3/4}} \frac{2R_{max}}{l} C_b$$

where

$$C_b = \frac{\gamma\sqrt{\pi}}{2^{3/4}\sqrt{\gamma+1}} \sqrt{\bar{I}_{max}} \quad (24)$$

RESULTS OF APPLICATION TO SPECIFIC BODIES

In order to investigate the effect of certain body-shape parameters upon the magnitude of the bow-shock overpressures, the body-shape constant C_b defined in equation (24) was evaluated for several families of body shapes by using equation (23). It should be remembered that C_b depends upon the cross-sectional-area distribution and, hence, is a function of such local details as nose angle and location of maximum thickness.

The first family of shapes was chosen to investigate the effect of varying the location of maximum thickness. The body shapes in this group for which the maximum thickness lies ahead of the center are shown in figure 3. By reversing these bodies, four shapes were obtained for which the maximum thickness lies behind the center. Since the nose angle varies as the location of maximum thickness is varied, the effect of the two parameters has not been completely isolated.

The effect of nose angle was investigated with the bullet-shape bodies of figure 4. The nose angles for these shapes vary from about 5° to 20°. The maximum thickness is held fixed at the base.
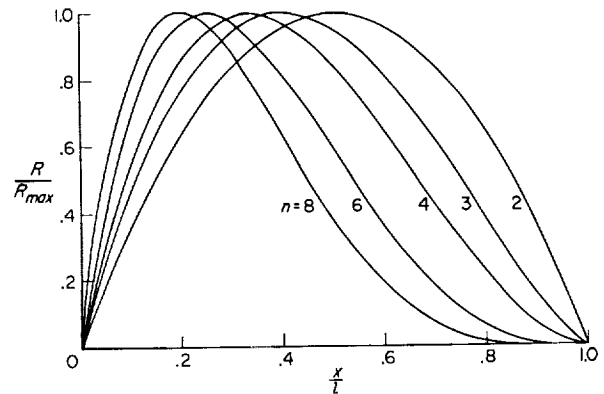

FIGURE 3.—Curves showing the radius of body shapes having various locations of maximum thickness.
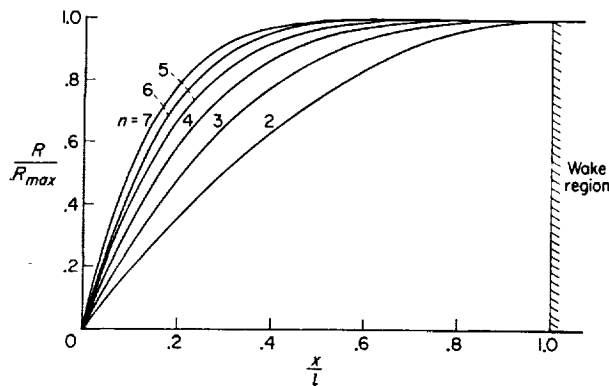
FIGURE 4.—Curves showing the radius of body shapes having various nose slopes.

By normalizing these shapes appropriately the group of body shapes shown in figure 5 are obtained. The nose angle is now constant, about 7°, and the maximum thickness is again fixed at the base; however, the fineness ratio varies from 8 to 28.

The shapes shown in figure 6 are similar to the shapes obtained at high Mach numbers by applying the supersonic area rule to actual airplane configurations. The forward portion of the shape is the same for all bodies and the location of the rearward hump is essentially fixed. Two shocks, one from the nose and another from the hump, contribute to the strength of the bow shock. The five shapes shown in figure 7 are equivalent bodies of revolution for actual airplane configurations. These body shapes are included for comparison with the idealized shapes treated elsewhere.

EFFECT OF LOCATION OF MAXIMUM THICKNESS

Figure 8 shows the variation of the body-shape constant for a family of shapes having various
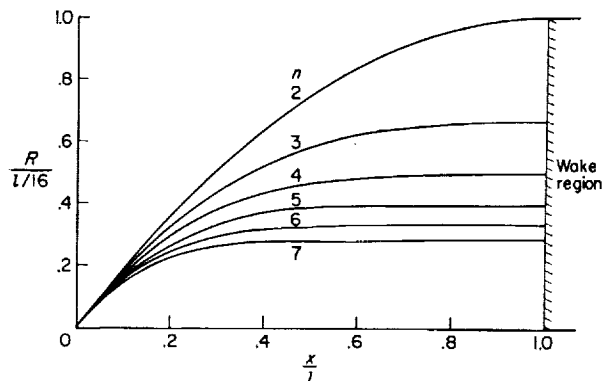

FIGURE 5.—Curves showing the radius of body shapes having various fineness ratios.
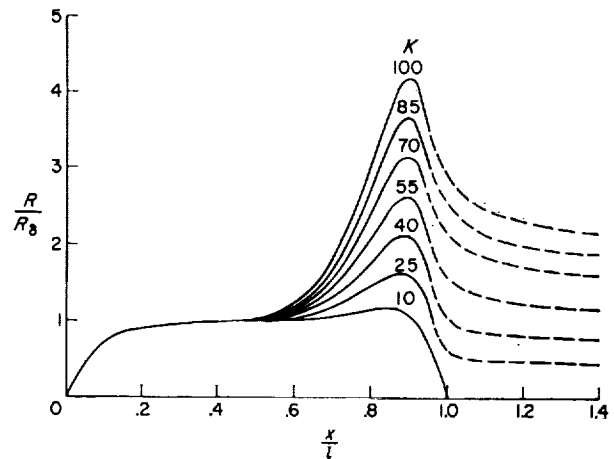

FIGURE 6.—Curves showing the radius of body shapes similar to those obtained from the supersonic area rule.
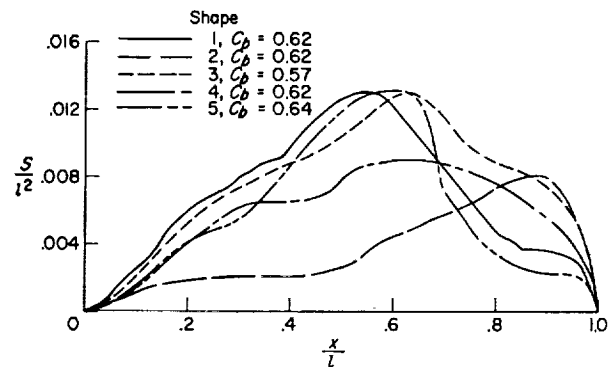

FIGURE 7.—Curves showing the radius of the equivalent bodies for several airplane configurations.
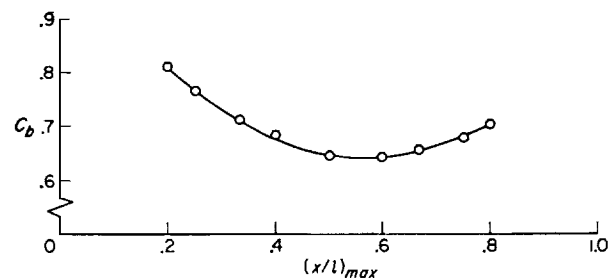

FIGURE 8.—Shape coefficient for bodies having various locations of maximum thickness.

locations of maximum thickness. The shapes for which the location of the maximum section is ahead of $x/l = 1/2$ are determined from the equation

$$\frac{R}{R_{max}} = A_1 \left(\frac{x}{l}\right) \left[1 - \left(\frac{x}{l}\right)^{n/2}\right] \qquad (25)$$

where $A_1 = \frac{n}{2}\left(1 + \frac{2}{n}\right)^{\frac{n}{2}+1}$. The constant A_1 nor-

malizes the right-hand side of the equation so that its maximum value on the interval $0 \leq \frac{x}{l} \leq 1$ is unity. The maximum cross section is located $(x/l)_{max} = 2/(2+n)$. These shapes are shown in figure 3. The shapes for which the maximum cross section is behind $x/l = 1/2$ are determined from the equation

$$\frac{R}{R_{max}} = A_1 \left(1 - \frac{x}{l}\right) \left(\frac{x}{l}\right)^{n/2} \qquad (26)$$

The location of the maximum section is given by $(x/l)_{max} = n/(2+n)$. The right-hand side of equation (26) is also normalized by A_1 so that its maximum value on the interval $0 \leq \frac{x}{l} \leq 1$ is unity. The shapes given by equation (26) are obtained by making the substitution $\frac{x}{l} = 1 - \frac{x}{l}$ in equation (25). Thus, for a fixed value of n the shape given by equation (26) is identical to that given by equation (25), but reversed in the flow. The wake assumed in the calculations is defined by $R_w = 0$. (Although the Von Karman drag is identical for two such reversed bodies, it is of interest to note that the sonic-boom pressure is different.)

Figure 8 shows that the body-shape constant C_b decreases by 20 percent as $(x/l)_{max}$ increases from 0.2 to 0.5. For the reversed shapes C_b increases as $(x/l)_{max}$ increases from 0.5 to 0.8. This increase is due to the extreme pointed nose. As $(x/l)_{max}$ increases, these shapes behave like bodies having a shorter length and a long thin probe pointed forward into the oncoming stream.

Since the nose angle for the nine shapes in this family varies with the location of maximum thickness the effects of these two parameters on the value of C_b have not been isolated.

EFFECT OF NOSE ANGLE AND FINENESS RATIO

The body shapes shown in figures 4 and 5 are determined from the equation

$$\frac{R}{R_{max}} = 1 - \left(1 - \frac{x}{l}\right)^n$$

In figure 4, $\frac{l}{2R_{max}} = 10$; this fixes the fineness ratio of the shapes, but allows the slope at the nose to vary according to the relation

$$R'(0) = \frac{n}{20}$$

In figure 5, $\frac{l}{2R_{max}} = 4n$. In this case the nose angle for all shapes is fixed at 7°, and the fineness ratio varies linearly with n. The body shapes as shown in figures 4 and 5 are considerably exaggerated in order to display more clearly their area development close to the nose. The wake for these shapes is taken to be a cylinder extending to an infinite distance downstream with a radius equal to that of the body base.

Figures 9 and 10 show a nearly linear increase in C_b with nose angle and fineness ratio. Although these two parameters vary by a factor of 3.5, the shape coefficient increases by only 20 percent. The increase in C_b in figure 9 represents an actual increase in the pressure jump due to increasing bluntness. However, the pressure jump associated with the shapes in figure 5 is proportional to $\frac{2R_{max}}{l} C_b = \frac{C_b}{4n}$ and decreases with increasing fineness ratio.

For the simple bullet-shape bodies shown in figures 9 and 5 the bow shock and the nose shock
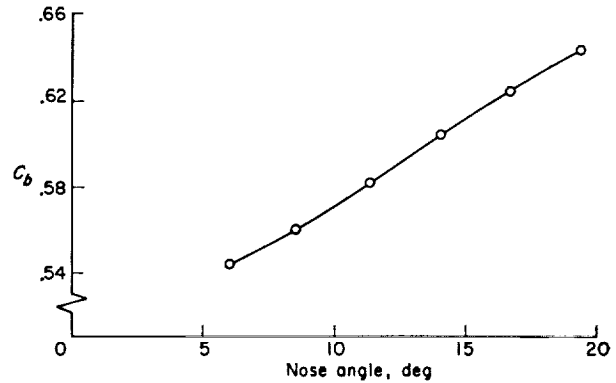

FIGURE 9.—Shape coefficient for bodies having various nose slopes.
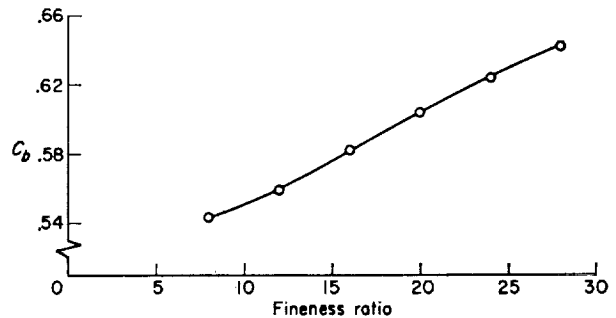

FIGURE 10.—Shape coefficient for bodies having various fineness ratios.

are identical. For more complicated configurations the bow shock may be a combination of several shocks which coalesce near the body. In such cases the nose angle may have even less effect upon the bow-shock overpressures than indicated in figure 9 as can be seen clearly for the next family of shapes discussed where the strength of the nose shock is a relatively small contribution to the total strength of the bow shock.

SOME SHAPES SIMILAR TO THOSE OBTAINED BY APPLYING THE SUPERSONIC AREA RULE

The body shapes shown in figure 6 have area distributions similar to those obtained at high Mach numbers by applying the supersonic area rule to actual flight configurations. The shapes were obtained from the equation

$$R=R_\delta\left[1-\left(2\frac{x}{l}-1\right)^6+K\left(1-\frac{x}{l}\right)\left(\frac{x}{l}\right)^{10}\right] \quad (27)$$

These shapes are quite flat in the region $0.3\leq\frac{x}{l}\leq0.5$.

The radius of the body in this region is denoted by R_δ. The important properties of these shapes are given in the following table:

K	$(x/l)_{max}$	$\frac{R_{max}}{R_\delta}$	$\left(\frac{l}{2R_{max}}\right)\left(\frac{R_\delta}{l}\right)$	$\left(\frac{l}{2R_{max}}\right)$ for $\frac{R_\delta}{l}=\frac{1}{84.4}$	$\overline{C}_b$
10	0.83	1.18	0.424	35.8	1.48
25	.87	1.64	.305	25.7	2.17
40	.89	2.15	.2325	19.6	3.05
55	.89	2.66	.188	15.9	3.95
70	.90	3.18	.1573	13.3	4.83
85	.90	3.70	.135	11.4	5.70
100	.90	4.22	.1185	10	6.57

As K increases, the location of the maximum cross section remains relatively fixed; however, the maximum radius increases by a factor of 4 for the range of K considered here. A given value of K fixes the value of the ratio $\frac{R_{max}}{R_\delta}$. The fineness ratio of the shape is then determined from the value of the fineness-ratio parameter $\left(\frac{l}{2R_{max}}\right)\left(\frac{R_\delta}{l}\right)$ once a value of $\frac{R_\delta}{l}$ is chosen. The wake used for each body in the calculations is shown as the broken curve in figure 6. It was chosen so that when $\frac{R_\delta}{l}=\frac{1}{84.4}$ the flow turns through an angle of $15°$ after passing over the peak. The flow then separates from the rear surface of the projectile and asymptotically approaches a cylinder of constant cross section. For $K=10$ the wake is simply $R_w=0$.

When $K>10$, the bow shock which extends into the far field from these shapes is a combination of two shocks—one from the nose and another from the steep incline ahead of the maximum cross section—which coalesce at some distance from the body. The nose shock has the same strength for all shapes; the strength of the second shock increases with R_{max}. Thus, if y_o in equation (15) were taken as the first root of $F(y)=0$ only the contribution of the nose shock would be taken into account.

In order to compare the relative strengths of the two shocks for a given body, it is convenient to introduce the parameter $\overline{C}_b=\left(\frac{2R_{max}}{R_\delta}\right)C_b$ so that $\frac{\Delta p}{p_\infty}=\frac{\beta^{1/4}}{\left(\frac{r}{l}\right)^{3/4}}\left(\frac{R_\delta}{l}\right)\overline{C}_b$. For a fixed value of $\frac{R_\delta}{l}$ all the bodies have the same nose shape ahead of $\frac{x}{l}=\frac{1}{2}$ and, hence, nose shocks of equal strength. The rearward hump gives rise to a second shock which augments the nose shock in the far field. The differences in the size and shape of the hump are responsible for the variation in $\overline{C}_b$. The values of $\overline{C}_b$ are given in the preceding table. When $K=10$ the bow shock and the nose shock are identical. By comparing $\overline{C}_b$ for $K=10$ with $\overline{C}_b$ for the other shapes it can be seen that the strength of the nose shock becomes less important as K increases. Thus, any changes in the strength of the nose shock due to changes in the nose shape of these bodies will be less significant than in those cases where the nose shock alone is responsible for the far-field pressure discontinuity.

Figure 11 again indicates only a small variation in the coefficient C_b in spite of the difference in the body shapes. In the present case there is a 20-percent decrease in C_b as the fineness ratio
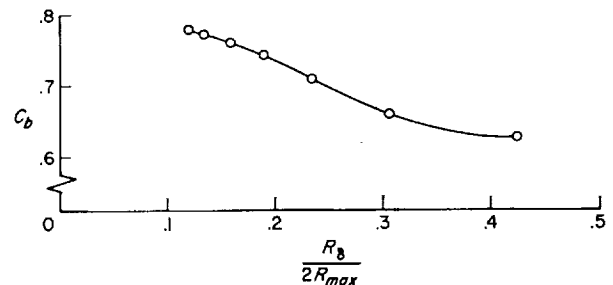

FIGURE 11.—Shape coefficient for bodies similar to supersonic-area-rule shapes.

varies by a factor of 3.5. This trend in C_b is the reverse of that shown in figure 10.

EFFECT OF THE WAKE

In order to investigate the flow field near the body close to and behind the base, Whitham's theory requires that some form be assumed for the shape of the wake. Pictures of projectiles in flight indicate that the wake turns roughly through 12° at the base and then converges to form a cylinder of nearly constant cross section equal to one-half the base area. Since the exact form of the wake is not specified, it is of interest to determine the effect of various wake shapes on the pressure rise across the shocks in the far field.

In order to investigate this question a shape obtained from equation (27) was used in which $K=55$ and $R_b/l=1/84.4$. Four different wake shapes were then considered as shown in figure 12. The first is a cylinder of constant cross section which joins smoothly to the maximum cross section of the body. The two intermediate wake shapes separate from the body after the flow has turned through 15° and 30°, respectively. At large distances behind the body these two shapes become asymptotic to cylinders of constant cross section. The fourth wake is defined by $S_w=0$, that is, the flow is tangent to the surface everywhere along the rear surface of the body. This requires the flow to turn through 38°.

The body-shape constant was calculated to be the same for all four wake shapes. This result is believed to hold in all cases where the wake separates from the body behind the maximum section and becomes thinner thereafter but no general demonstration can be given. The strength of the tail shock, however, is affected by the shape of the wake as shown in reference 1.
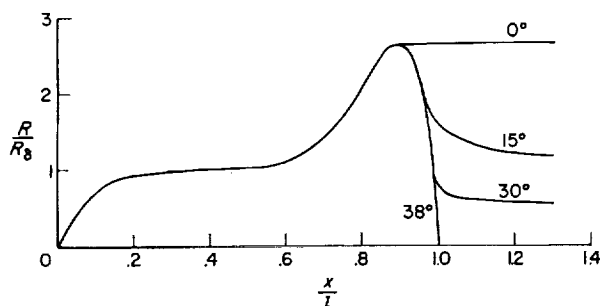

FIGURE 12.—Curve showing the radius of a body shape with various assumed wakes.

SEVERAL AIRPLANE AREA DISTRIBUTIONS

References 4 and 9 indicate that the sonic-boom pressures associated with a nonaxisymmetric airplane configuration may be predicted from Whitham's theory by replacing the actual area distribution by an equivalent body of revolution obtained from the supersonic area rule. Whitham's method has recently been extended to lifting configurations in another manner which is also based on an "equivalent body" concept (ref. 10). The five shapes shown in figure 7 are equivalent-body area distributions for actual airplane configurations. These shapes have a rather irregular area development and are included for comparison with the smooth shapes treated previously.

Shape 2 is a Mach number 3 supersonic area distribution which is similar to the shapes in figure 6. The other four shapes (1, 3, 4, and 5) are Mach number 1 area distributions. The bow shocks on shapes 1, 2, and 3 are a combination of three shocks which appear ahead of $(x/l)_{max}$, whereas the bow shocks for shapes 4 and 5 are a combination of two shocks. In spite of the diversity of the local details of these five shapes C_b again changes very little and the pressure jump is largely determined by the fineness ratio.

CONCLUSIONS

The physical implications of the basic hypothesis for Whitman's modification of linear theory (Communications on Pure and Applied Mathematics, August 1952) have been considered and a brief derivation given of the far-field equations for the bow shock. An integral which determines the effect of body shape upon the bow-shock overpressures in the far field has been reduced to a form which involves only the cross-sectional-area distribution and can be readily evaluated for body shapes for which no analytical expression is available. The integral has been evaluated for a number of families of body shapes chosen to investigate the effects of nose angle, fineness ratio, and location of maximum cross section on the bow-shock overpressures. The results of these calculations indicate the following conclusions:

1. In regard to body geometry, the pressure discontinuity in the far field is, to a first order, independent of body shape and depends only on

the fineness ratio. Local details have second-order effects which, in general, can be accounted for only by direct computation of the body-shape constant.

2. The calculated values of the shape constant which determines the effect of body geometry upon the pressure jump varied from 0.54 to 0.81.

A convenient value of the shape constant is 0.64, but an accurate determination of this constant should be made if a careful comparison between theory and experiment is desired.

LANGLEY RESEARCH CENTER,
  NATIONAL AERONAUTICS AND SPACE ADMINISTRATION,
    LANGLEY FIELD, VA., *March 29, 1960.*

REFERENCES

1. Whitham, G. B.: The Flow Pattern of a Supersonic Projectile. Communications on Pure and Appl. Math., vol. V, no. 3, Aug. 1952, pp. 301–348.
2. Friedrichs, K. O.: Formation and Decay of Shock Waves. Communications on Appl. Math., vol. I, no. 3, Sept. 1948, pp. 211–245.
3. DuMond, Jesse W. M., Cohen, E. Richard, Panofsky, W. K. H., and Deeds, Edward: A Determination of the Wave Forms and Laws of Propagation and Dissipation of Ballistic Shock Waves. Jour. Acous. Soc. of America, vol. 18, no. 1, July 1946, pp. 97–118.
4. Carlson, Harry W.: An Investigation of Some Aspects of the Sonic Boom by Means of Wind-Tunnel Measurements of Pressures About Several Bodies at a Mach Number of 2.01. NASA TN D-161, 1959.
5. Maglieri, Domenic J., Hubbard, Harvey H., and Lansing, Donald L.: Ground Measurements of the Shock-Wave Noise From Airplanes in Level Flight at Mach Numbers to 1.4 and at Altitudes to 45,000 Feet. NASA TN D-48, 1959.
6. Mullens, Marshall E.: A Flight Test Investigation of the Sonic Boom. AFFTC-TN-56-20, Air Res. and Dev. Command, U.S. Air Force, May 1956.
7. Daum, Fred L., and Smith, Norman: Experimental Investigation of the Shock Wave Pressure Characteristics Related to the Sonic Boom. WADC-TN-55-203, U.S. Air Force, Aug. 1955.
8. Liepmann, H. W., and Roshko, A.: Elements of Gasdynamics. John Wiley & Sons, Inc., c.1957.
9. Walkden, F.: The Shock Pattern of a Wing-Body Combination, Far From the Flight Path. Aero. Quarterly, vol. IX, pt. 2, May 1948, pp. 164–194.
10. Ryhming, I. L., and Yoler, Y. A.: Supersonic Boom of Wing-Body Configurations. Paper No. 60-20, Inst. Aero. Sci., Jan. 1960.